Validation and sensitivity test of the distributed hydrology soil-vegetation model (DHSVM) in a forested mountain watershed

Enhao Du,[1]* Timothy E. Link,[2] John A. Gravelle[3] and Jason A. Hubbart[4]

[1] *Climate Science Department, Lawrence Berkeley National Lab, One Cyclotron Road–84R0171, Berkeley, CA 94720-8268, USA*
[2] *College of Natural Resources, University of Idaho, 875 Perimeter Drive MS 1133, Moscow, ID 83844-1133, USA*
[3] *Environmental Sciences Graduate Program, University of Idaho, Morrill Hall 216, Moscow, ID 83844-3006, USA*
[4] *Department of Forestry, University of Missouri, Columbia, 1105 E. Rollins, 203-Q ABNR Building, Columbia, MO 65211, USA*

Abstract:

Hydrologic models are often calibrated and validated with streamflow from a limited number of sites, whereas assessment of model performance with internal watershed data can be used to constrain the parameterization of physically based models to verify that specific hydrologic processes are being reasonably simulated. This is particularly important for improving the simulation accuracy of models used to evaluate potential hydrologic responses to land use and climate change. The distributed hydrology soil-vegetation model (DHSVM) was parameterized for the Mica Creek Experimental Watershed in northern Idaho. Performance was assessed based on measured streamflow from nested and paired watersheds, snowpack dynamics, soil moisture, and transpiration estimated from sap flux. In general, DHSVM effectively simulated snowpack dynamics, soil water content, and the streamflow regime. Streamflow simulation for seven subcatchments had model efficiencies ranging between 0.63 and 0.79. Model efficiency of snowpack simulation at a SNOTEL site was 0.95. Some minor discrepancies between simulated and measured values suggested that some processes, such as snow redistribution, were not represented by the model or were insufficiently parameterized for local conditions. A sensitivity analysis indicated that soil porosity, leaf area index, and minimum stomatal resistance were among the most influential parameters that affected variations in the simulated hydrological regime. However, those variables can be reasonably estimated based on field or remote sensing data. Other important parameters, such as saturated hydraulic conductivity, are more difficult to quantify and therefore need to be refined during the calibration phase. A description of the iterative parameter refinement process that was used in the calibration phase of the model is included to assist other researchers in refining model parameterizations. Copyright © 2013 John Wiley & Sons, Ltd.

KEY WORDS   watershed hydrology; DHSVM; validation; sensitivity test; continental/maritime climate

Received 12 June 2013; Accepted 8 November 2013

INTRODUCTION

Physically based hydrologic models typically include a detailed representation of physical processes across digital elevation model (DEM) grids or hydrologic response units. Despite this detail, model performance is frequently assessed based on comparisons between simulated and measured streamflow and snow water equivalent (SWE) because these variables are often collected as part of operational water monitoring programmes. Spatially distributed internal watershed states and fluxes are not commonly assessed because of challenges of data collection in remote forested mountainous terrain. Notable exceptions include studies by Whitaker (2003) and Thyer *et al.* (2004) that assessed the accuracy of the distributed hydrology soil-vegetation model (DHSVM) to simulate internal watershed variables including radiation transfer, snow dynamics, canopy interception, soil moisture, and transpiration, and Fang *et al.* (2013) who completed a multi-variable assessment of a hydrological simulation using the Cold Regions Hydrological Modelling platform. These studies are valuable because a number of processes contribute to the streamflow regime, and errors in simulated processes may effectively counteract each other, thereby generating reasonable flow simulations despite internal errors. This can result in equifinality where a number of parameter sets could achieve equally reasonable simulations (Beven, 1993).

Performance accuracy of physically based hydrologic models depends on adequate specification of a large number of parameters; however, states and/or fluxes of interest may only be sensitive to a small subset. Many parameters are difficult to measure or estimate and, hence, have to be specified within physically meaningful bounds by informed trial and error during the calibration process.

*Correspondence to: Enhao Du, Climate Science Department, Lawrence Berkeley National Lab, One Cyclotron Road–84R0171, Berkeley, CA 94720-8268, USA.
E-mail: duleisi@hotmail.com

It is very important for a modeller to understand the degree of influence that different parameters and driving variables have on simulated hydrologic quantities. Sensitivity analyses can provide mechanistic insight to hydrologic processes, which can help focus measurement and estimation efforts and can assist in the manual calibration process to provide a basis and direction of adjustment when automatic calibrations are not feasible, thereby improving confidence in simulated effects of land cover change on hydrologic states and fluxes (Gooseff *et al.*, 2005; Bahremand and Smedt, 2008).

To ensure that distributed hydrologic models can be used with confidence to evaluate cover change effects on watershed hydrology, model validation with internal, spatiotemporally varying hydrologic quantities is necessary. In addition, simple sensitivity tests are also needed as an alternative of Monte Carlo simulations to help constrain and prioritize measurements of key model parameters. The primary objective of this study is therefore to evaluate the performance and sensitivity of DHSVM for hydrologic simulation of a 4th-order stream system located in a snow-dominated mountainous watershed with a range of land cover conditions. The specific technical questions are to assess the following: (1) the simulation accuracy of internal watershed components including snowpack, soil water content (SWC), transpiration, and sub-watershed streamflows, and (2) the sensitivity of the simulated flow regime to model parameters. Study outcomes include information to help researchers determine

model strengths and weaknesses and parameterization strategies to correctly simulate hydrologic responses to land cover and climate changes.

METHODS

Study site

The Mica Creek Experimental Watershed (MCEW) is located in northern Idaho at 47.17°N latitude, 116.27°W longitude. The watershed is composed of an area approximately 28 km^2 (Figure 1) and ranges in elevation from 1000 to 1600 m. Average annual precipitation is approximately 1400 mm per year, with roughly two thirds occurring as snow between October and March. The average annual air temperature is approximately 5 °C. Soils formed *in situ* from material weathered from schist and quartzite bedrock with a mantle of volcanic ash and a duff layer and are typically deep and well drained. Hillslopes typically range in steepness from 15% to 30%. Second-order and greater stream gradients range from 3% to 14%. Vegetation at the MCEW consists of 80- to 90-year-old mixed conifers regenerated from extensive logging in the early 1930s. A mixture of tree species is found in the watershed, with the majority composed of grand fir (*Abies grandis*), Douglas-fir (*Pseudotsuga menziesii*), western red cedar (*Thuja plicata*), and western larch (*Larix occidentalis*). Stands average 75% crown closure, and average canopy heights are roughly 30 m.
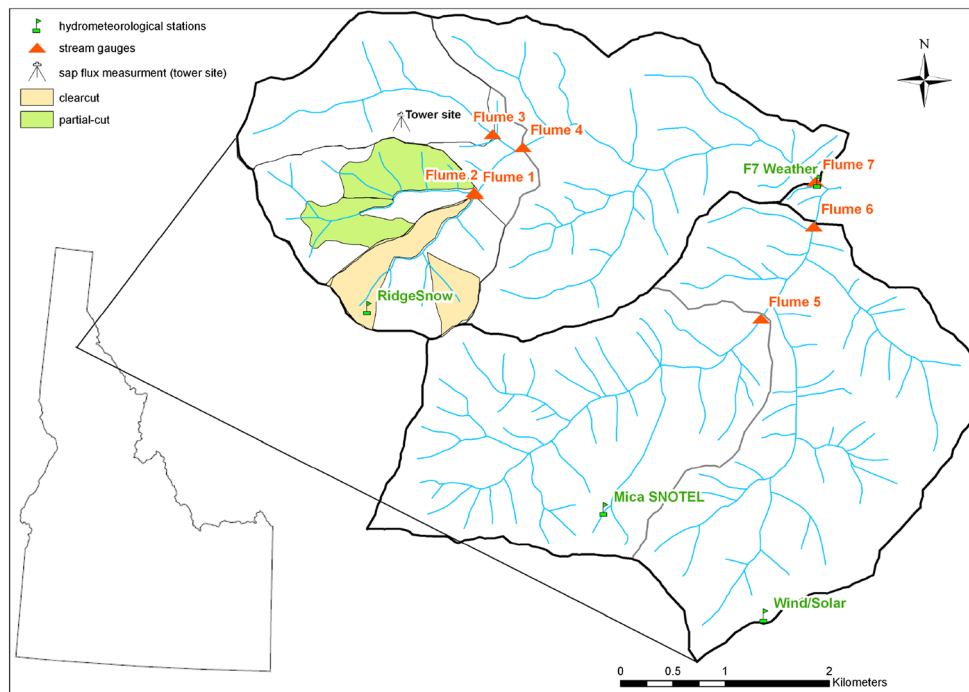
Figure 1. Map of the Mica Creek Experimental Watershed study area in northern Idaho showing locations of the stream gauging stations, Mica Creek SNOTEL site, and hydrometeorological stations

These physiographic, climatic, and vegetative characteristics are typical of many forested watersheds in the interior Pacific Northwest where extensive harvest occurs.

The Mica Creek study was designed to evaluate the cumulative effects of timber harvest using a before–after, control–impact paired series experimental design (Stewart-Oaten *et al.*, 1986) consisting of paired and nested gauged watersheds (Figure 1). The watershed was logged and burned in the 1930s and sustained limited anthropogenic impacts until 1997 when roads were constructed for timber harvest activities. The fraction of roads in the study area is roughly 2–3% (Karwan *et al.*, 2007). In 2001, after a 4-year post-road period, two forested headwater drainages on the West Fork Mica Creek (Catchments 1 and 2) were harvested to assess the effects of contemporary harvest practices. In Catchment 1, 50% of the drainage area was clear cut, whereas in Catchment 2, 50% of the drainage area was partial cut with 50% of the canopy cover removed (such that 25% of the canopy was removed). A third headwater drainage on the West Fork (Catchment 3) was left intact as a climatic control unit (Gravelle and Link, 2007; Hubbart *et al.*, 2007b).

Data collection

The Mica Creek SNOTEL station located at 1372 m amsl provided air temperature, precipitation, and SWE on a daily basis since 1990 (Figure 1). Shortwave (0.28–3.5 µm) radiation and longwave (3.5–100 µm) radiation were measured with a LI-200 pyranometer (LI-COR Corporation, Lincoln, Nebraska) since 1997 and pyrgeometer (Kipp&Zonen Inc., Delft, the Netherlands) since 2004, respectively, at the Wind/Solar meteorological station located on an exposed ridge on the southern boundary of the catchment. Wind speed data were recorded using a cup anemometer (MetOne Instruments Inc., Grants Pass, OR, USA). Air temperature and relative humidity were measured with a Vaisala HMP45C combination temperature/relative humidity sensor (Vaisala Corporate, Finland) installed in a Gill radiation shield since 2004. All hydrometeorological data were recorded as 15-min averages on attached data loggers (CR10X, Campbell Scientific Inc., Logan, UT, USA).

Throughfall was measured in 2004 using arrays consisting of 20 bulk throughfall collection buckets and 20 tipping bucket rain gauges (TE-525I, Texas Electronics Inc., Dallas, TX, USA) equipped with individual data loggers (HOBO Event, Onset Computer Corp., Bourne, MA, USA) that were installed in open, control, and thinned forested areas. Data from the tipping bucket arrays were used to derive canopy storage parameters according to the methods described by Link *et al.* (2004b). Leaf area index (LAI) was measured with a LAI-2000 plant canopy analyzer

(LI-COR Corporation, Lincoln, Nebraska) in June and July 2007. Sap flux was measured on eight trees within a 100 m radius around the Tower Site (Figure 1) to estimate transpiration and to derive canopy conductance values. Sap flux was monitored with radial sap flow metres (Granier, 1987) at 10-min intervals from June through October 2006, and May through October 2007, respectively.

Stream discharge was measured at 30-min intervals at seven gauging stations consisting of a Parshall flume with a nitrogen bubbler-type pressure transducer system (Riverside Technology Inc., Fort Collins, CO, USA). Specific rating curves for each flume were determined from measured stage–discharge relationships and were recalibrated annually (Hubbart *et al.*, 2007a). Snow surveys were conducted weekly along 14 snow courses during the winter of 2006 from accumulation phase (before peak SWE) through complete ablation. Transects were 20 m long and stratified by treatments (control, partial cut, and clear cut) and aspects. Snow depth and SWE values were recorded every 2 and 4 m, respectively, using a standard Mt Rose snow tube and a spring balance.

Soil water content sensors (ECH$_2$O, Decagon Devices Inc., Pullman, WA, USA) were installed at depth increments of 15 cm down to 90 or 105 cm, depending on the presence of rocks in the soil (Figure 1). The probes were attached to a Campbell CR10X data logger at meteorological stations MC100, MC200, and MC300 (Figure 2), and measurements were recorded every 30 min for water years 2005 and 2006. Sensors were calibrated *in situ* based on gravimetric analysis of soil samples collected in the immediate vicinity of the profiles spanning a wide range (0.19–0.55 vol vol^{-1}) of moisture conditions. In addition, 14 sets of stainless steel waveguides of 25, 50, and 75 cm in length were randomly located throughout the study area, stratified by forest treatment. These SWC readings were collected with a portable TDR unit (6050X3K1 Mini Trase, SoilMoisture Equipment Corp., Santa Barbara, CA, USA), every 2 to 4 weeks during the snow-free period from May through November in 2005 and 2006.

Distributed hydrology soil-vegetation model

The DHSVM (Wigmosta *et al.*, 1994) is a physically based, spatially distributed hydrological model that explicitly solves the mass and energy balance equation at the pixel scale. The model has been successfully applied to evaluate hydrologic effects of logging (Storck *et al.*, 1998; Bowling *et al.*, 2000; VanShaar *et al.*, 2002; Schnorbus and Alila, 2004; Thanapakpawin *et al.*, 2006) and forest road construction (Bowling and Lettenmaier, 2001; LaMarche and Lettenmaier, 2001; Waichler *et al.*, 2005) in a variety of forested watersheds. DHSVM was shown to be suitable to simulate land cover changes
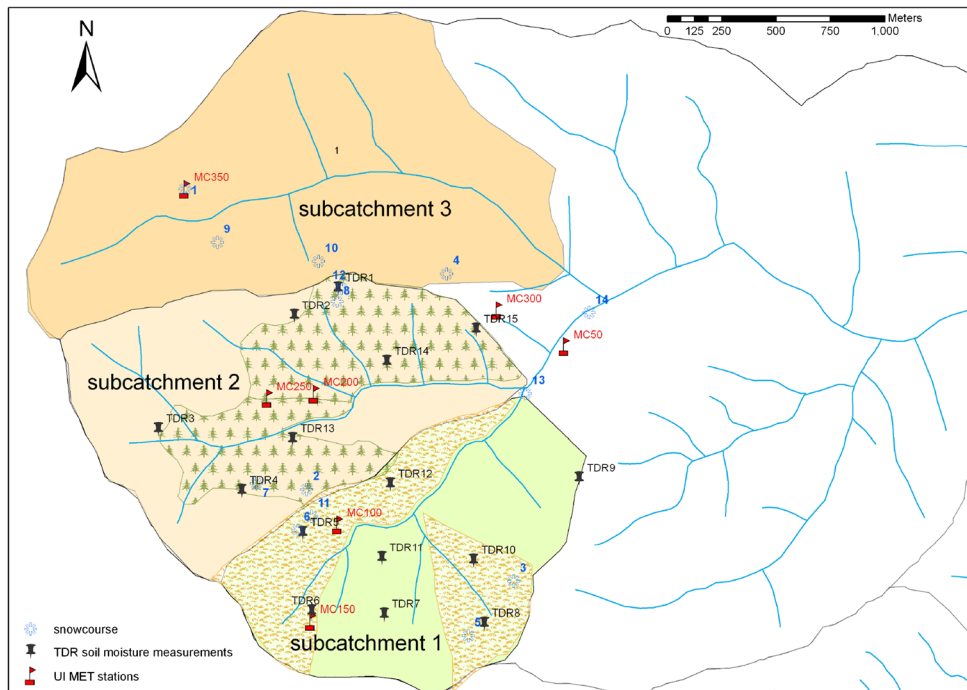
Figure 2. Map of the Mica Creek Experimental Watershed Subcatchments 1–4, showing locations of meteorological, soil moisture, and snowpack monitoring sites

owing to its explicit representation of energy exchanges and evaporation and transpiration (ET) algorithms (VanShaar *et al*., 2002). The version employed in this study was 2.0.1 released in November 2007.

Spatial and hydrometeorological data preparation

Model grid size was 30 m, thereby conforming to the base 30-m DEM acquired from the U.S. Geological Survey National Mapping programme. Vegetation classification

was derived from the Idaho GAP Analysis Project (Caicco *et al*., 1995) prior to treatment. The forest cover types used in the model were primarily evergreen conifer and mixed conifer (evergreen and deciduous conifers) classes with minor amounts of riparian forest, shrub-dominated, and other classes (Table I). Field measurements indicated that LAI values ranged from 6 to 8 for most of the canopy conditions, so the summer LAI for the majority of classes (evergreen and mixed conifer) was set to 7.5. Winter LAI was adjusted according to the composition of the stands

Table I. Land cover classifications

	Overstory LAI		Understory LAI		
	Summer	Winter	Summer	Winter	Percent area (%)
Evergreen conifer	7.5	7.5	0.2	0.1	64.10
Deciduous conifer	7	5.3	0.2	0.1	0.45
Broadleaf	6	2.5	0.2	0.1	0.09
Mixed conifer	7.5	6	0.2	0.1	28.48
Needleleaf riparian	7.5	7	0.3	0.1	0.62
Broadleaf riparian	7.5	2	0.3	0.1	0.12
Mixed riparian	7.5	5.5	0.3	0.1	0.09
Non-forest riparian	0	0	1	0.1	0.25
Shrub	0	0	1.5	0.1	0.24
Evergreen partial cut	3.8	3.8	0.3	0.1	0.70
Mixed partial cut	3.8	3	0.3	0.1	2.37
Clear cut	0	0	0.2	0.1	2.45

Note: LAI, leaf area index.

(Table I). The canopy height was specified as 30 m based on the mean value determined from an acquisition of high-resolution (<2 m) light detection and ranging (LiDAR) data processed using a multi-scale curvature classification algorithm (Evans and Hudak, 2007). Soil types were derived from the Soil Survey Geographic database and were represented by the Boulder Creek series. The stream network was generated using the flow routing module in the ArcGIS software package based on the 30-m DEM. Topographic shading maps were derived based on sun angle and the surrounding topography (Frew, 1990) on the 15th day of every month at the temporal resolution of the model (i.e. 3 h in this study).

Three-hour values of precipitation were derived from the daily record at the Mica Creek SNOTEL station and evenly distributed across each day. Three-hour average air temperatures were interpolated from daily maximum and minimum air temperatures from the Mica Creek SNOTEL station using a 3-point spline method (Akima, 1978). Hydrometeorological variables from the Wind/Solar station on the southern watershed boundary were used when available. Incoming shortwave radiation prior to 1997 was calculated based on solar geometry and geographic location using Image Processing Workbench modelling tools (Frew, 1990). The daily atmospheric transmittance was estimated from the magnitude of the diurnal temperature range (Bristow and Campbell, 1984), with the minimum value set to 0.1. Longwave radiation was estimated from air temperature using the Stefan–Boltzmann equation, where atmospheric emissivity was computed as a function of air temperature and vapour pressure (Brutsaert, 1975). Shortwave radiation after 1997 and longwave radiation after 2004 were measured at the Wind/Solar station and were used directly to drive the model.

Relative humidity data were estimated for the simulation period prior to 2004 using a modified method based on the mean daily potential evapotranspiration rate as an index of vapour pressure (Kimball et al., 1997). Wind data prior to 1997 were acquired from a previous study in which wind speeds were generated from the NCEP/NCAR Reanalysis Project (VanShaar, 2002). The wind series was extracted from the lowest model layer at 75 m and scaled to the reference height at 36 m assuming an exponential velocity profile (equivalent to 6 m above the 30-m-high canopy). After 1997, wind speed was monitored at the Wind/Solar meteorological station, located at a height of 6 m on an open ridge, and assumed to represent conditions at 6 m above the forest canopy.

Parameterization and calibration

Parameters used to represent the vegetation canopy and soils for the DHSVM simulations are listed in Table II. Values were either measured at the site or estimated

based on values obtained from the primary literature wherever possible to limit calibration. Parameters related to soil properties and stomatal mechanics were refined to improve the simulation of streamflow and soil moisture dynamics. As a result, the model required relatively minimal calibration, with parameter values constrained by the best understanding of the physically based components that govern hydrologic states and fluxes in the watershed.

The minimum canopy resistance was derived from sap flux measurements in 2006. Values were plotted against vapour pressure deficit (VPD) and the value estimated by the y-intercept of a fitted exponential decay function (Pangle, 2008). The minimum canopy resistance was then multiplied by LAI to obtain the minimum stomatal conductance (R_{sm}) value of $680 \, s \, m^{-1}$. The sap flow-estimated R_{sm} was relatively high compared with other values in the literature that ranged from 70 to $500 \, s \, m^{-1}$ (Kelliher et al., 1993; Dingman, 1994; Schulze et al., 1994; Link et al., 2004a), but was considered to be reasonable for the 70- to 80-year-old conifer forest at this site. Analysis of high temporal resolution throughfall data (Link et al., 2004b) indicated that the canopy saturation storage was roughly 2.0 mm for rain; therefore, the multiplier for intercepted precipitation was set to 0.0003 mm per LAI to approximate this value. Canopy interception capacity for snowfall (when converted to snow water equivalent) was set to equal the rainfall value. Tree rooting depths were set to 0.9 m based on analyses of soil pits nearby trees and continuous water content data that indicated relatively constant values below this depth, as depths shallower than this exhibited greater seasonal variations, indicative of water extraction by roots. The threshold above which soil moisture does not restrict vegetation transpiration is estimated to be half of the field capacity for old-growth trees (Leaf and Brink, 1975).

For the soil parameterization, only the Boulder Creek series was used for the model because the two soil types are very similar except for a different textural composition in the lower layers. The physical soil properties acquired from the USDA NRCS STATSGO database included estimates of saturated hydraulic conductivity, clay content, and field capacity. Soil saturated lateral hydraulic conductivity (SLHC) was estimated by a weighted average of each layer and was refined during calibration. Bubbling pressure and pore size distribution were estimated based on soil texture values from the primary literature (Tables 5.3.2 and 5.3.3 in Maidment (1992)). The values of porosity, field capacity, and wilting point were refined based on a combination of measured soil properties and SWC, and were set to 0.60, 0.45, and $0.05 \, vol \, vol^{-1}$ for the upper layer, compared with the lower layer that was set to 0.47, 0.39, and $0.11 \, vol \, vol^{-1}$ for the three parameters, respectively. During the calibration phase, the hydraulic conductivity

Table II. Calibrated constants and parameters

Description	Reference value
Global constants	
Bare ground aerodynamic roughness	0.02 m
Snow surface aerodynamic roughness	0.01 m
Multiplier for leaf area index (LAI) to determine intercepted rain/snow	0.0003/0.0003
Soil parameters	
Saturated lateral hydraulic conductivity (SLHC)	1.5×10^{-4} (%)
Exponent for lateral conductivity decrease with depth (decrease exponent)	3
Maximum infiltration rate	3×10^{-5} (m s^{-1})
Soil surface albedo	0.1
Porosity (1st, 2nd, and 3rd layers)	0.65/0.51/0.50
Pore size distribution (PSD) index (1st, 2nd, and 3rd layers)	0.24/0.24/0.24
Bubbling pressure (1st, 2nd, and 3rd layers)	0.5/0.11/0.1 (bar)
Field capacity (1st, 2nd, and 3rd layers)	0.48/0.43/0.26
Wilting point (1st, 2nd, and 3rd layers)	0.06/0.09/0.17
Bulk density (1st, 2nd, and 3rd layers)	700/1400/1400 (kg m^{-3})
Vertical saturated conductivity (1st, 2nd, and 3rd layers)	3×10^{-5}/3.1×10^{-7}/4.8×10^{-7} (m s^{-1})
Dry soil thermal conductivity (1st, 2nd, and 3rd layers)	7.114/6.923/6.923 (W m^{-3} °C^{-1})
Soil thermal capacity (1st, 2nd, and 3rd layers)	1.4×10^{6}/1.4×10^{6}/1.4×10^{6} (J m^{-3} °C^{-1})
Vegetation parameters	
Overstory maximum snow interception capacity	0.04
Ratio of mass release to meltwater drip from snow interception	0.3
Aerodynamic attenuation coefficient for wind calculation	3.9
Radiation attenuation by the overstory canopy	0.46
Snow interception efficiency	0.6
Maximum stomatal resistance (overstory/understory)	3000/1000 (s m^{-1})
Minimum stomatal resistance (overstory/understory)	680/300 (s m^{-1})
Soil moisture threshold to restrict evaporation and transpiration (ET; overstory/understory)	0.18/0.16
Vapour pressure deficit (VPD) threshold above which stomata close (overstory/understory)	4000/4000 (Pa)
Photosynthetically active shortwave radiation (RPC, overstory/understory)	0.108/0.108
One-sided overstory leaf area index	Varies among species
Overstory albedo	0.1

was increased by up to one order of magnitude to reasonably reproduce the magnitude and shape of the peak flows, which may be explained by the contribution of macropore flow that is not explicitly implemented in the version of the model that was used. This is in accordance with findings from similar forested (Thyer *et al.*, 2004) and agricultural (Brooks *et al.*, 2004) settings.

Assessment of the streamflow calibration was divided to two phases both of which were based on 3-h resolution data. In the first phase from 1992 to 1997, shortwave and longwave radiation, wind speed, and relative humidity were modelled rather than measured as described earlier (Figure 3). In the second phase from 1998 to 2007, all driving meteorological data were measured at the site. The Nash–Sutcliffe model efficiency (NSE) for the simulated streamflow during the first stage was 0.57, and the percent root mean square difference (PRMSD) was 1.02, whereas for the second stage, NSE was 0.72 and PRMSD was 0.66. The mass balance error was −3.1% for the first stage and −11.5% for the second stage. Seasonal statistics

indicated that the model performed relatively well during the snow melt seasons (NSE = 0.84) but has larger discrepancies in the fall (NSE = 0.38) when the model does not accurately represent peak flows resulting from rain events during the transitional wetting phase.

Sensitivity analysis

A local sensitivity test (Cacuci, 2003) using stepwise, single parameter perturbation approach of model constants, plant physiological parameters, and soil parameters (Table II) for the 2002 to 2007 time period was completed by systematically varying key parameters and determining the effect on simulated water yield, 5th percentile flows (upper 5% of annual flow volume) as an index of high flow regime, and half-mass date (the date when half of the annual flow volume has passed the gauge). These three indices were selected because they are frequently of interest in investigations focused on the effects of changing land covers on flow regimes. A global sensitivity test with
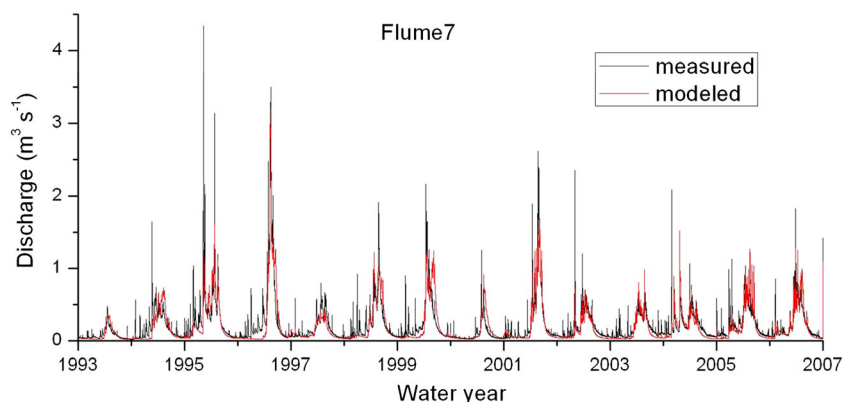
Figure 3. Measured and modelled streamflow for 1993–2007

randomly selected parameter values (e.g. Monte Carlo simulation) is more desirable. However, the simulation involves thousands of model runs (Surfleet *et al.*, 2010) and requires enormous computational capability, which is not readily available in many cases. The 5th percentile flow was selected as an index of high flow regime over instantaneous peak flows. This is because large peak flows in the interior Pacific Northwest typically are triggered by rain-on-snow events (MacDonald and Hoffman, 1995), and simulation of instantaneous peaks depends on highly accurate characterizations of canopy conditions, soil properties, and meteorological variables and hence may be very sensitive to small errors in a number of these quantities.

The parameters tested comprise most constants and coefficients required by the model except temperature and precipitation lapse rates, trunk space, fraction coverage of vegetation, mass release dripping ratio, root zone depth, and all understory coefficients. Each parameter was varied by the following multipliers to produce 11 separate cases: 0.1, 0.25, 0.5, 0.8, 0.9, 1.1, 1.2, 2, 4, and 10, plus the baseline value that was determined by model calibration unless the product exceeded the limits set by the model or was physically meaningless. The offset values were selected to have a finer resolution close to the base values (e.g. 0.9/1.1, 0.8/1.2, 0.5/2, and 0.25/4) and extend to an order of magnitude change above and below the base value. Any parameter in the top third of the sensitivity ranking for any of three indices was categorized as having high sensitivity; the middle third was classified as moderate, and the lowest third as low.

RESULTS AND DISCUSSION

Model validation

Streamflow. Refinement of parameters that control the hydrograph was based on flows for Catchment 7, which comprised the northern half of the study watershed. The objective of the overall Mica Creek project is to effectively simulate and understand differences in hydrologic dynamics related to land cover differences; hence, model validation was based on performance in catchments with different physiographic and land cover conditions. Therefore, the same parameterization that was developed for Catchment 7 was applied to Subcatchments 1–4 and the adjacent Catchments 5 and 6 that comprised the southern half of the study area for the same preharvest (1993–2001) and postharvest (2002–2007) periods, respectively. For the preharvest period, streamflow simulations for Subcatchments 1–4 that comprised the headwaters of Catchment 7 exhibited comparable performance, with NSE ranging between 0.71 and 0.79 and annual yield differences ≤5%, with the exception of Subcatchment 3 yield that was overestimated by roughly 12% (Table III). The NSE were slightly less (0.7 and 0.69, respectively) in Catchments 5 and 6, but were still within an acceptable range. The model underestimated the runoff by approximately 11% in Catchment 6, compared with the underestimate of 2% in Catchment 7. For the postharvest period (2002–2007), the NSE for Subcatchments 1, 2, and 4, and Catchment 7 (in which treatments took place) were 0.63, 0.74, 0.72, and 0.74, respectively. Measured and modelled streamflows exhibited reasonable agreement both before and after the 2001 treatments that occurred in Subcatchments 1 and 2.

The high flow simulation exhibited relatively good agreement with the measurements in Catchment 7 where the modelled 5th percentile streamflows were overestimated by 9%. The streamflow simulation successfully replicated the spring snowmelt peak flows but underestimated some of the small peak flows generated by fall storm events as noted earlier. This discrepancy is likely due to there being no explicit representation of shallow subsurface lateral flow in the model that was not completely overcome by the proxy provided by the specific hydraulic conductivity parameter settings. Another source of discrepancies is the methods used to disaggregate precipitation from daily to 3-h time steps and estimate air temperature from daily maximum

Table III. Subcatchment preharvest simulation statistics

Subcatchment	1	2	3	4	5	6	7
Nash–Sutcliffe efficiency	0.76	0.70	0.74	0.79	0.70	0.69	0.76
Percent root mean square difference	0.70	0.83	0.82	0.75	0.90	0.85	0.76
Water yield difference (%)	−1.5	+5.2	+12.3	+1.5	+6.9	+10.5	+2.0

and minimum values (Safeeq and Fares, 2011). Based on the results by Waichler and Wigmosta (2003), these sources of error are expected to be relatively minor in this environment, because convective precipitation events are of minor importance and cold season precipitation is almost entirely composed of snowfall; hence, precipitation phase estimation is relatively insensitive to air temperature errors caused by the interpolation method.

Snowpack dynamics. The SWE simulation matched measurements at the SNOTEL site very well (Figure 4) with an NSE of 0.93, PRMSD of 0.46%, and absolute mean bias difference of 0.001 m for the 1993–2007 snow seasons. The good agreement was expected at this site because much of the hydrometeorological driving data were collected at this location. Data from the 14 snow courses were used to further assess the performance of the snow simulations in 2006. Overall, DHSVM reasonably simulated the snowpack dynamics at most of the snow survey points (Figure 5). The largest SWE underestimates occurred at snow courses #7, #13, and #14. Of these sites, #7 was in the partial cut canopy but traversed a broad skid trail with minimal canopy interception capacity. Sites #13 and #14 were located in the valley bottom in a closed canopy forest consisting of old-growth western red cedar (*Thuja plicata*). The gaps between trees in this area were much larger than in the second-growth forests, and snow courses #13 and #14 generally traversed the middle of the gaps; hence, the SWE was relatively high at all sites because of less canopy interception. The simulated SWE

was relatively consistent throughout the clear-cut areas, whereas the measurements displayed more variability, and SWE was notably overestimated at snow course #6. Snow course #6 was located near the top of a slope break, and it appears that snow was locally redistributed to a more sheltered topographic concavity immediately downslope. These cases illustrate why it is critical to carefully evaluate measurement locations before using limited data to calibrate or validate models because the simulation of snowpack dynamics was generally reasonable with the exception of these locations.

When comparing SWE simulations by canopy treatment, both the model and measurements indicated that the clear-cut areas accumulated the most snow, relative to the partial cut and control forested areas. The clear-cut areas also exhibited some of the larger discrepancies relative to the measured values that were likely due to spatial variability caused by redistribution and/or preferential deposition that were not simulated by DHSVM. The second-growth closed canopy and partial cut forests, however, exhibited more consistent agreement between the modelled and simulated dynamics, likely due to the lack of snow drifting in these areas. Whitaker *et al.* (2003) attributed the snowpack simulation residual in their study to misrepresentation of spatial patterns of meteorological inputs. This may be another potential source of error in the current work. Overall, snowpack dynamics in the different land cover classes were effectively simulated by the model despite some discrepancies that appear to be associated with incorrect
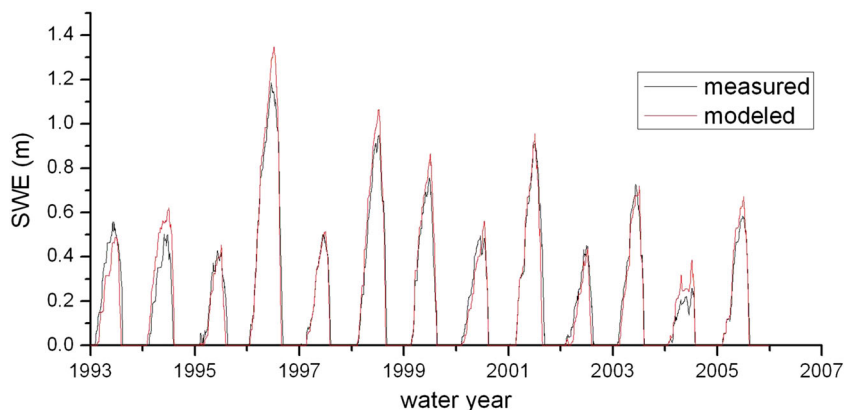
Figure 4. Comparison of snow water equivalent (SWE) measured at the Mica SNOTEL site to distributed hydrology soil-vegetation model simulated SWE. Nash–Sutcliffe model efficiency was 0.93, and percent root mean square difference was 0.46
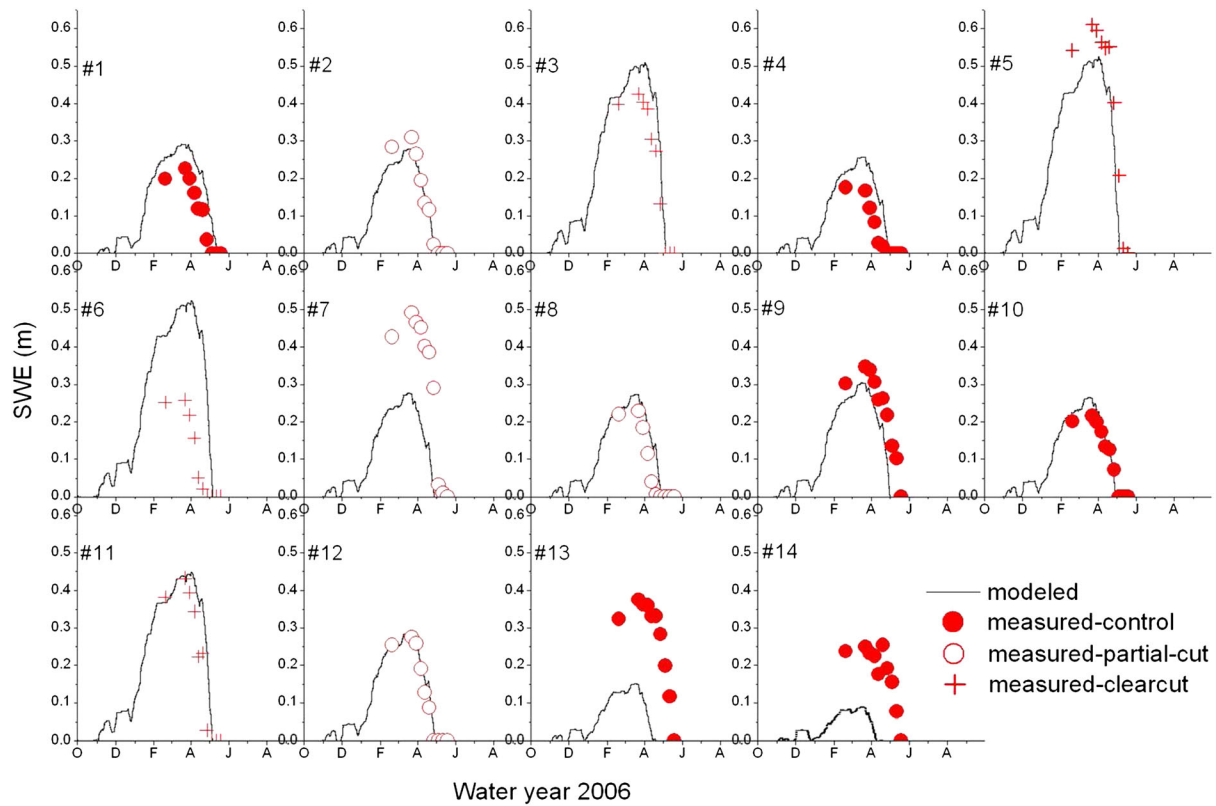
Figure 5. Measured and modelled snow water equivalent (SWE) during the 2006 winter within the three primary land cover classes at the 14 snow courses (forcing data from Hubbart and Link, in prep)

assumptions regarding the overlying canopy and lack of redistribution and/or preferential deposition processes in the model.

Soil water content. The SWC simulations were compared with continuous measurements from a meteorological station (MC200) under a partial cut forest canopy (Figure 6) as an example and at 14 locations across the study
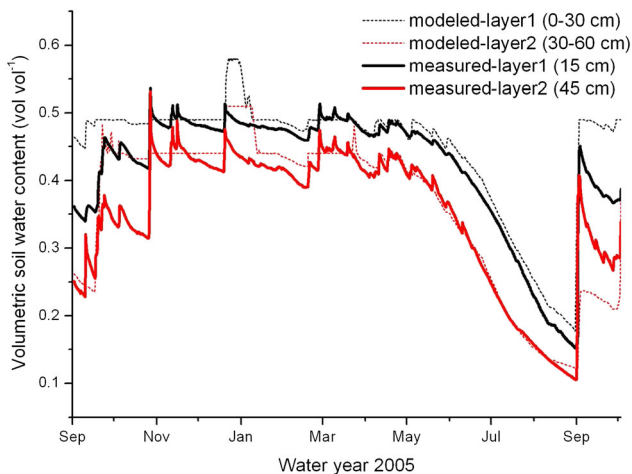
Figure 6. Measured and modelled volumetric soil water contents for shallow and deep soil layers at the MC200 meteorological station

catchments where manual measurements were made in 2006 (Figure 7). The soil moisture simulation at the MC200 site is provided as an example of continuous soil moisture simulation performance, and results were similar at the other two sites. The modelled values exhibited very good agreement with the measurements in the top two layers (Figure 6), considering the high degree of spatial variation in soil properties that can occur over very short distances (Hillel, 1998). The measured SWC trends in both soil layers in late spring and summer were very well replicated by the simulated trends, implying that the soil-vegetation component of the hydrological cycle was reasonably simulated at the grid cell.

The spatially distributed SWC measurements clustered around the primary drying and re-wetting period (June–October) because of lack of access to the probes during the period of snow cover. Because the soil properties are highly heterogeneous over the spatial scale of a grid cell, it is almost impossible for the model to represent all of the variations, and hence, it is more important to verify that the model reproduced the relative dynamics rather than the absolute values. The SWC simulations at the 14 measurement points generally captured the seasonal dry-down trend and replenishment of SWC in the fall (Figure 7). At several locations (e.g. #5, #6, #8, #10, and #12), the absolute SWC values
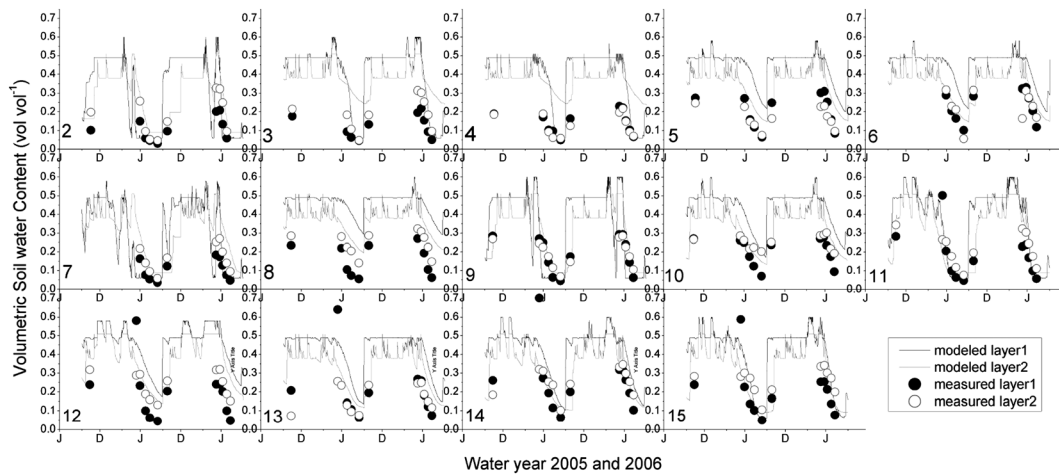
Figure 7. Measured and modelled soil water content (sensor set #1 was missing). Sites 5, 6, 7, 8, and 12 are located in the clear-cut patch and are likely affected by reduced soil water storage capacity as a result of soil compaction and/or incorrect evaporation and transpiration representation. Layer 1 spans the 0–30 cm depth; modelled layer 2 spans the 30–60 cm depth; measured layer 1 is approximately 0–25 cm depth; measured layer 2 is approximately the 25–45 cm depth average

showed considerable discrepancies between the measured and simulated values. These sensors were all located in the clear-cut patches covered by a thin grass layer (LAI = 0.2) in the model representation. The simulated SWC reflected the land cover differences with much larger values throughout the entire season, whereas the TDR measurements displayed much smaller changes (mostly in the lower layer) relative to other treatments. The discrepancies are possibly caused by a combination of errors in the land cover and/or shallow soil parameters and localized differences between the scale of the simulations (10s of m) and measurements (~0.1 m). The SWC comparisons were included in the validation as a general assessment of model performance that was deemed to be reasonable for the purpose of simulating the effects of land cover change on streamflow regimes despite some noted absolute differences between the modelled and measured values.

Sap flux. Transpiration (T) estimated from sap flux measurements and the sum of ET fluxes computed by DHSVM are plotted in Figure 8. DHSVM combines transpiration and evaporation fluxes into one output term. There were relatively large discrepancies between estimated T from sap flux and modelled ET values in the spring months, likely due to evaporative losses of canopy-intercepted water. This is supported by the large discrepancies that occurred immediately following very low flux values corresponding to periods of precipitation when evaporation of canopy-intercepted water would be expected to be very large. One notable exception is the highly variable simulated ET signal relative to the more damped sap flux signal around day 210. The reason for these differences may be due to tree capacitance effects
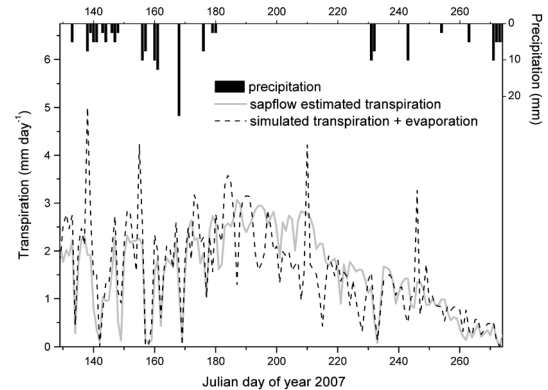
Figure 8. Simulated transpiration + evaporation compared with transpiration estimated based on sap flow measurements. Discrepancies, especially in the early season, are likely due to evaporation of canopy-intercepted water from precipitation events

that are not simulated by the model but that were observed in comparisons between basal and canopy sap fluxes (Pangle, 2008).

After the onset of the seasonal drought toward the end of June, ET was relatively high when both SWC and air temperatures were high. Later in the season, low SWCs and high VPDs became constraining factors; hence, ET progressively declined for the remaining summer months. The measured and modelled fluxes exhibited better agreement during the summer months, when precipitation declined and fluxes were primarily dominated by transpiration. The simulated evapotranspiration also showed reasonable agreement with the lower values on the sap flow estimated transpiration curve where evaporation of intercepted water was not expected to contribute to the total ET flux. Thyer *et al*. (2004) found the opposite in that simulated ET was underestimated

when rainfall was present and interpreted the discrepancy to be caused by an underestimation of low evaporation rate of intercepted rain.

The general consistency between the simulated ET and measured sap flow as a transpiration estimate is an important component indicating that reasonable ecophysiological parameters were selected for the modelling application. This is especially important when models are used to assess the hydrologic consequences of land use alteration. Even though estimates of T derived from measurements of sap flux were compared with simulated ET fluxes, the general evaporative flux trends were well represented by the model. Thus, the parameterization appeared to be effective for this system, suggesting that the model should be an effective tool for assessing the hydrologic effects associated with land cover changes.

Model sensitivity

In total, there were 10 high sensitivity parameters, 10 moderate sensitivity parameters, and 10 low sensitivity parameters (Table IV). As expected, in this system, the annual water yield was strongly affected by ET, whereas high flows and half-mass dates were influenced mainly by snowmelt dynamics. Based on the sensitivity rankings, responses of streamflow variables for a range of parameter alterations were plotted for changes in the top 10 influential parameters. In Figures 9–11, the x-axis indicates parameter perturbations ranging from a factor of 0.10 to 10 times the base value, and y-axis indicates the normalized responses for annual water yield, 5th percentile flows, and half-mass date, respectively. Points that plot farthest from the x-axis indicate a high degree of sensitivity, whereas points that plot close to the x-axis for a wide range of changes indicate a very low degree of sensitivity.

Streamflow was moderately sensitive to 10 of the parameters assessed. For example, the snow interception
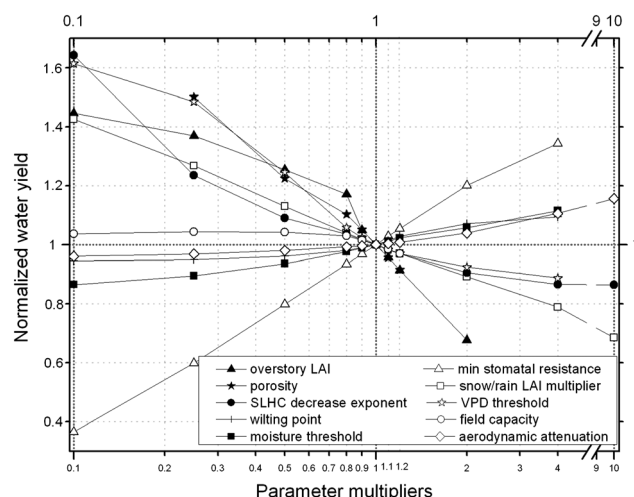
Figure 9. Sensitivity results for water yield. Only the 10 most sensitive parameters are shown. Large vertical offsets indicate a relatively high sensitivity to the given parameter. SLHC, saturated lateral hydraulic conductivity; VPD threshold, vapour pressure deficit threshold above which stomata close; moisture threshold, soil moisture threshold to restrict ET; aerodynamic attenuation, aerodynamic attenuation coefficient for wind calculation; LAI, leaf area index. See Table II for description of the parameters

efficiency only produced an 8% change in runoff volume over a change of two orders of magnitude. The radiation and aerodynamic attenuation coefficients affected the half-mass date but had a relatively small impact on the annual water yields and high flow regimes. Incident shortwave radiation is partitioned into overstory intercepted and transmitted radiation by the canopy radiation attenuation coefficient (τ_0). When τ_0 increases, the snowpack receives less energy input and the snowmelt rate drops, and therefore, the half-mass date advances (Figure 11). The aerodynamic attenuation coefficient (n_a) is used in the model to calculate the aerodynamic resistance of the surface. When n_a is increased, the wind speed is more attenuated at the ground, the snow melt rate consequently decreases, and hence the half-mass date

Table IV. Relative sensitivity rankings

High	Moderate	Low
Overstory leaf area index (LAI) (−)	Radiation attenuation (−)	Bubbling pressure
Min stomatal resistance (+)	Aerodynamic attenuation (±)	Snow roughness
Porosity (−)	Overstory albedo (+)	Bulk density
Snow/rain LAI multiplier (−)	RPC (+)	Ground roughness
Exponential decrease (−)	Snow interception efficiency (±)	Max infiltration rate
Saturated lateral hydraulic conductivity (SLHC) (+)	Snow water capacity (−)	Soil albedo
Vapour pressure deficit (VPD) threshold (−)	Pore size distribution (PSD) (+)	Thermal capacity
Wilting point (+)	Vertical conductivity (+)	Thermal conductivity
Field capacity (−)	Max resistance (+)	Dripping ratio
Moisture threshold (+)	Max snow interception capacity (−)	Min intercepted snow

Note: The parameters are ranked in terms of general importance, although the ranking is not absolute as the relationships are not linear. The plus and minus signs indicate whether the runoff volume is positively or negatively related to the variable change; the '±' sign indicates a bowl-like water yield relationship curve. See Table II for detailed parameter descriptions.
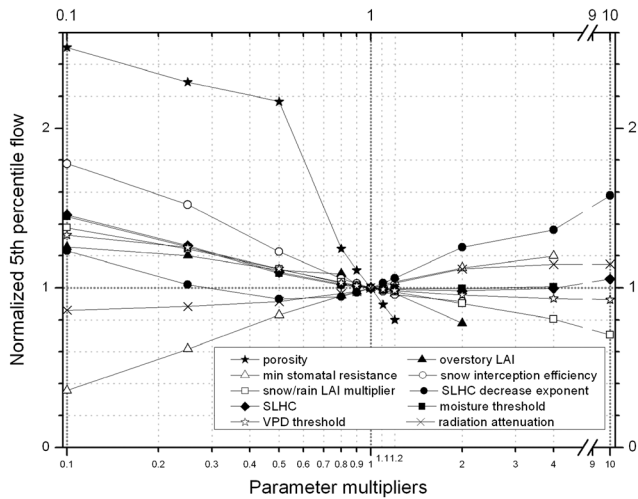
Figure 10. Sensitivity test results for 5th percentile streamflows. The response list is slightly different from that by water yield, whereas porosity and minimum resistance are still on top of the ranking. SLHC, saturated lateral hydraulic conductivity; VPD threshold, vapour pressure deficit threshold above which stomata close; moisture threshold, soil moisture threshold to restrict ET; LAI, leaf area index; radiation attenuation, radiation attenuation by the overstory canopy
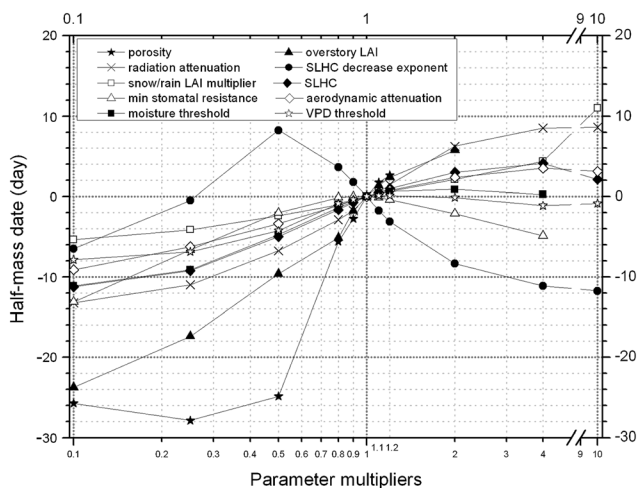
Figure 11. Sensitivity test results for the half-mass date. *Y*-axis indicates number of days that half of the annual water yield advances as a result of altering each parameter. Negative values indicate earlier runoff, whereas positive values indicate later runoff. SLHC, saturated lateral hydraulic conductivity; VPD threshold, vapour pressure deficit threshold above which stomata close; moisture threshold, soil moisture threshold to restrict ET; aerodynamic attenuation, aerodynamic attenuation coefficient for wind calculation; LAI, leaf area index

advances. It is also important to note that some of the parameters do not vary greatly in nature, such as overstory albedo, liquid water holding capacity of the snow, and the soil moisture threshold; thus, the combination of low natural variability and relative insensitivity suggests that these parameters can be reasonably estimated based on values from the literature.

Sensitivity test results indicated that streamflow regimes are very sensitive to variations in LAI. This is because LAI directly affects three key hydrological processes: evaporation and sublimation of canopy-intercepted precipitation, transpiration of soil water, and snowpack energetics, specifically the radiative and turbulent heat fluxes. In DHSVM, LAI is used as a multiplier in precipitation interception, canopy conductance, and turbulent energy flux attenuation calculations. In this study, only overstory LAI (i.e. tree LAI) was tested, because the shrub and herbaceous leaf areas usually comprise a minor proportion of the total LAI. With higher LAIs, trees intercept more precipitation and transpire more water. Therefore, the overstory LAI is inversely related to water yield (Figure 9). In the energy balance calculations, shortwave radiation is transmitted according to Beer's Law (Wigmosta *et al.*, 2002), which is an exponential function that includes LAI. Higher LAIs result in less radiation reaching the ground so the snowmelt rate is reduced. Combined with less SWE accumulation, higher overstory LAIs result in reduced high flows and delayed runoff (Figures 10 and 11). The flow regime was also very sensitive to the snow/rain LAI multiplier that controls the canopy interception storage capacity and the minimum stomatal resistance (R_{sm}) that affects transpiration. Flow regimes were sensitive to the VPD threshold parameter, defined as the VPD above which stomatal closure begins to occur, and the moisture threshold parameter, which is the SWC above which transpiration, is unrestricted.

The flow regimes were sensitive to a number of parameters that characterize subsurface storage and flow characteristics. When soils with low porosity and/or infiltration capacity receive a relatively small amount of water, excess water in the model is converted to overland flow that is routed to the channel system much faster than subsurface flow. The half-mass date is therefore sensitive to porosity and occurs earlier as porosity decreases. For the same reason, a porosity decrease causes more spring snowmelt to be converted to streamflow that otherwise would have been retained by the soil, and therefore, high flows were very sensitive to this parameter as shown by the steep response curve in Figure 10. Porosity affects ET and hence influences the runoff volume. As the soil water characteristic curve remains the same, soils with high porosity can store more water that is readily available for plant uptake, and therefore, in these simulations, the water yield decreased with increasing porosity.

Annual water yield was found to be sensitive to the field capacity and wilting point that constrain the upper and lower bounds of the plant available water, respectively. The high flow regime is sensitive to both the SLHC and the exponential decrease coefficient (e_d) that describes the change in the SLHC with depth. This is

because DHSVM only simulates lateral subsurface water movement when soil layers are saturated. Peak flows are usually composed of a combination of baseflow (saturated flow), shallow subsurface lateral flow through macropores in the unsaturated soils, and overland flow. Shallow subsurface lateral flow is not included in the version of DHSVM used in this investigation, so only saturated flow and overland flow (which rarely occurs in this environment) are simulated. The SLHC and e_d may cause saturated lateral flow velocities to increase or decrease such that they may be either synchronized or desynchronized from different parts of the catchment; therefore, high flows do not exhibit a consistent response to changes in these parameters.

In summary, many of the parameters that drive DHSVM model sensitivity can be directly measured or derived from other measurements, including LAI, wilting point, field capacity, VPD threshold, snow/rain LAI multiplier, and snow interception efficiency. This makes the model parameterization relatively easy to constrain, especially for detailed studies where the research focus is on coupled hydrological and ecological processes. Minimum stomatal resistance can be estimated from porometer measurements at the leaf scale or from sap flow measurements at the individual tree scale. The VPD and soil moisture threshold can be estimated from relationships between transpiration–VPD and transpiration––SWC where such data exist. Aerodynamic and radiation attenuation coefficients are usually derived from literature values based on vegetation characteristics because these parameters are harder to determine empirically. This approach is acceptable for most applications except for extreme rain-on-snow flood events that are strongly affected by high wind speeds, because key annual and seasonal flow regime variables also exhibit relatively low sensitivity to these parameters.

Implications for model calibration

Here, we summarize a brief description of implications for the manual calibration process based on the procedure employed in this research and results of the sensitivity tests, in order to assist other researchers with the calibration of physically based models such as DHSVM in similar environments. As many parameters as possible should be constrained by field measurements, especially the ones in high sensitivity group. Soil physical properties can be estimated by (1) sampling and laboratory analyses of soils at multiple locations and depths to determine the water characteristic function, and (2) continuous soil moisture monitoring to estimate rooting depth and field capacity. LAI can be estimated and mapped from ground-based measurements and/or remotely sensed data products such as airborne LiDAR.

The canopy interception coefficient can be estimated by measuring rain and/or snow under the canopy and comparing with measurements in the open, or from values in the literature. Saturated hydraulic conductivities (K_{sat}) are usually more difficult to quantify, partly owing to large spatial heterogeneity and extensive macropore networks in forests. R_{sm} is another difficult parameter to estimate spatially given the potential errors of scaling measurements up from single sap flow probes to an entire watershed. As a result, both K_{sat} and R_{sm} are the two primary parameters that were used in this research to refine the model parameterization.

Once initial parameters are estimated, model performance can be evaluated based on three major output indices: water balance, high flows, and baseflows. Reasonable approximation of the water balance based on the streamflow record is the initial step, followed by refinement of the parameters that control the high and low flow regimes, and finally further refinement of the water balance because modification of the parameters that control flow regimes often result in degradation of the water balance simulation. Soil storage and K_{sat} largely control the high flow regime, and small soil storage and high K_{sat} values generate flashy peak flows. Once the high flow is well represented in the model (e.g. proper magnitude and temporal duration), the baseflow can be adjusted primarily with the R_{sm}, VPD threshold, and moisture threshold that in combination affect transpiration. R_{sm} is the main parameter that can be adjusted to reflect water use by vegetation. Soil depth and field capacity are not included in this parameterization but are key variables that determine soil water storage. Normally, high K_{sat}, small soil storage, and high R_{sm} would induce lower baseflows. After high flows and baseflows are reasonably matched with the hydrograph, minor refinement of parameters such as LAI and R_{sm} that affect the water balance is usually needed. The parameter refinement is an iterative process among all three indices, because an adjustment of one index frequently adversely affects others, whereas the ultimate goal is to maximize the accuracy of all three indices. Manual calibration of DHSVM is also a labour-intensive process but may be streamlined by focusing on a reduced set of parameters that the model is most sensitive to based on the results of the sensitivity analysis provided earlier.

SUMMARY AND CONCLUSIONS

This research indicated that, in general, DHSVM reasonably simulated snowpack, SWC, transpiration, and streamflow dynamics both before and after clear and partial cut harvesting. There are some discrepancies that reveal issues that may not have been identified had not the detailed internal data been collected. Snow redistribution and/or preferential deposition are not simulated by the model but

appear to be responsible for some of the discrepancies. Although the snow simulation was very good at the SNOTEL site, the model did not accurately represent locations in small canopy gaps that receive relatively large amounts of snow but small amounts of net radiation. Soil moisture simulations at the continuously monitored profile sites agreed very well with observed data, and in general, spatial patterns were reasonably represented. The model effectively simulated transpiration dynamics during the growing season when evaporation of intercepted rainfall was unlikely to occur. One should be critical of both the scale and site location of internal watershed data, as not all measurements may be representative of conditions over modelling grid cells.

Local sensitivity analyses were performed by a perturbation-response method. Thirty model parameters were categorized into three sensitivity groups as producing high, moderate, and low streamflow responses. Overstory LAI, minimum stomatal resistance, and soil porosity along with seven other parameters were found to be the most influential. Many of the sensitive parameters can be constrained by direct measurements, but some parameters (e.g. SLHC) still need to be refined during model calibration because of spatial heterogeneity. It should be noted that these analyses were specific to a snow-dominated environment characterized by moderately steep slopes and coniferous canopies but nonetheless provide insight into potential model sensitivity at other sites. Overall, DHSVM reasonably simulated streamflow, snowpack, SWC, and transpiration dynamics for a range of canopy conditions typical of second-growth managed forestlands. This calibrated version of the model hence can be used with confidence to assess the impact of land cover alterations and climate changes on hydrologic regimes.

REFERENCES

Akima H. 1978. A method of bivariate interpolation and smooth surface fitting for irregularly distributed data points. *ACM Transactions on Mathematical Software* **4**: 148–159.

Bahremand A, Smedt FD. 2008. Distributed hydrological modeling and sensitivity analysis in Torysa Watershed, Slovakia. *Water Resources Management* **22**: 393–408.

Beven K. 1993. Prophecy, reality and uncertainty in distributed hydrologic modeling. *Advances in Water Resources* **16**: 41–51.

Bowling LC, Lettenmaier DP. 2001. The effects of forest roads and harvest on catchment hydrology in a mountainous maritime environment. In *The Influence of Land Use on the Hydrologic–Geomorphic Responses of Watersheds*, Wigmosta MS, Burges SJ (eds). Water Resources Monograph Series, American Geophysical Union: Washington, DC; 145–164.

Bowling LC, Storck P, Lettenmaier DP. 2000. Hydrologic effects of logging in Western Washington, United States. *Water Resources Research* **36**: 3223–3240.

Bristow KL, Campbell GS. 1984. On the relationship between solar radiation and daily maximum and minimum temperature. *Agricultural and Forest Meteorology* **31**: 159–166.

Brooks ES, Boll J, McDaniel PA. 2004. A hillslope-scale experiment to measure lateral saturated hydraulic conductivity. *Water Resources Research* **40**: W04208.

Brutsaert W. 1975. On a derivable formula for long-wave radiation from clear skies. *Water Resources Research* **11**: 742–744.

Cacuci D. 2003. *Sensitivity and Uncertainty Analysis*. Chapman and Hall/CRC: Boca Raton, Florida.

Caicco SL, Scott JM, Butterfield B, Csuti B. 1995. A gap analysis of the management status of the vegetation of Idaho (U.S.A.). *Conservation Biology* **9**: 498–511.

Dingman SL. 1994. *Physical Hydrology*. Prentice-Hall, Inc.: Upper Saddle River, New Jersey.

Evans JS, Hudak AT. 2007. A multiscale curvature algorithm for classifying discrete return LiDAR in forested environments. *IEEE Transactions on Geoscience and Remote Sensing* **45**: 1029–1038.

Fang X, Pomeroy JW, Ellis CR, MacDonald MK, Debeer CM, Brown T. 2013. Multi-variable evaluation of hydrological model predictions for a headwater basin in the Canadian Rocky Mountains. *Hydrology and Earth System Sciences* **17**: 1635–1659.

Frew JE. 1990. The image processing workbench. In *Geography*. University of California: Santa Barbara; 305.

Gooseff MN, Bencala KE, Scott DT, Runkel RL, Mcknight DM. 2005. Sensitivity analysis of conservative and reactive stream transient storage models applied to field data from multiple-reach experiments. *Advanced Water Resources* **28**: 479–492.

Granier A. 1987. Evaluation of transpiration in a Douglas-fir stand by means of sap flow measurements. *Tree Physiology* **3**: 30.

Gravelle JA, Link TE. 2007. Influence of timber harvesting on headwater peak stream temperatures in a Northern Idaho Watershed. *Forest Science* **53**: 189–205.

Hillel D. 1998. *Environmental Soil Physics*. Academic Press: San Diego, CA; 771.

Hubbart J, Link TE, Gravelle JA, Elliot WJ. 2007a. Timber harvest impacts on water yield in the continental/maritime hydroclimatic region of the United States. *Forest Science* **53**: 169–180.

Hubbart JA, Kavanagh KL, Pangle R, Link TE, Schotzko A. 2007b. Cold air drainage and modeled nocturnal leaf water potential in complex forested terrain. *Tree Physiology* **27**: 631–639.

Karwan DL, Gravelle JA, Hubbart JA. 2007. Effects of timber harvest on suspended sediment loads in Mica Creek, Idaho. *Forest Science* **53**: 181–188.

Kelliher FM, Leuning R, Shulze E-D. 1993. Evaporation and canopy characteristics of coniferous forests and grasslands. *Oecologia* **95**: 153–163.

Kimball JS, Running SW, Nemani R. 1997. An improved method for estimating surface humidity from daily minimum temperature. *Agricultural and Forest Meteorology* **85**: 87–98.

LaMarche JL, Lettenmaier DP. 2001. Effects of forest roads on flood flows in the Deschutes River, Washington. *Earth Surface Processes and Landforms* **26**: 115–134.

Leaf CF, Brink GE. 1975. Land use simulation model of the subalpine coniferous forest zone. *USDA Forest Service Research Paper RM-135, U.S. Department of Agriculture, Washington, D.C.*

Link TE, Flerchinger GN, Unsworth M, Marks D. 2004a. Simulation of water and energy fluxes in an old-growth seasonal temperate rain forest using the simultaneous heat and water (SHAW) model. *Journal of Hydrometeorology* **5**: 443–457.

Link TE, Unsworth M, Marks D. 2004b. The dynamics of rainfall interception by a seasonal temperate rainforest. *Agricultural and Forest Meteorology* **124**: 171–191.

MacDonald LH, Hoffman JA. 1995. Causes of peak flows in northwestern Montana and northeastern Idaho. *Water Resources Bulletin* **31**: 79–95.

Maidment DR. 1992. *Handbook of Hydrology*. McGraw-Hill Inc.: New York.

Pangle RE. 2008. Transpiration and canopy conductance of mixed species conifer stands in an inland Pacific northwest forest. In *Department of Forest Resources*. University of Idaho: Moscow; 199.

Safeeq M, Fares A. 2011. Accuracy evaluation of ClimGen weather generator and daily to hourly disaggregation methods in tropical conditions. *Theoretical and Applied Climatology* **106**: 321–341.

Schnorbus M, Alila Y. 2004. Forest harvesting impacts on the peak flow regime in the Columbia Mountains of South-eastern British Columbia: an investigation using long-term numerical modeling, 38.

Schulze E, Kelliher FM, C. Korner, J. Lloyd, Leuning R. 1994. Relationships among maximum stomatal conductance, ecosystem surface conductance, carbon assimilation rate, and plant nitrogen nutrition: a global ecology scaling exercise. *Annual Review of Ecology and Systematics* **25**: 629–660.

Stewart-Oaten A, Murdoch WW, Parker KR. 1986. Environmental impact assessment: "pseudoreplication" in time? *Ecology* **67**: 929–940.

Storck P, Bowling L, Wetherbee P, Letternmaier D. 1998. Application of a GIS-based distributed hydrology model for predication of forest harvest effects on peak stream flow in the Pacific Northwest. *Hydrological Processes* **12**: 889–904.

Surfleet CG, Skaugset AE, McDonnell JJ. 2010. Uncertainty assessment of forest road modeling with the distributed hydrology soil vegetation model (DHSVM). *Canadian Journal of Forest Research* **40**: 1397–1409.

Thanapakpawin P, Richey J, Thomas D, Rodda S, Campbell B, Logsdon M. 2006. Effects of landuse change on the hydrologic regime of the Mae Chaem river basin, NW Thailand. *Journal of Hydrology* **334**: 215–230.

Thyer M, Beckers J, Spittlehouse D, Alila Y, Winkler R. 2004. Diagnosing a distributed hydrologic model for two high-elevation forested catchments based on detailed stand- and basin-scale data. *Water Resources Research* **40**: 1029–1049.

VanShaar JR. 2002. *Effects of Land Cover Change on the Hydrologic Response of the Pacific Northwest Forested Catchments*. Department of Civil and Environmental Engineering, University of Washington: Seattle, Washington; 187.

VanShaar JR, Haddeland I, Lettenmaier DP. 2002. Effects of land-cover changes on the hydrological response of interior Columbia River basin forested catchments. *Hydrological Processes* **16**: 2499–2520.

Waichler SR, Wigmosta MS. 2003. Development of hourly meteorological values from daily data and significance to hydrological modeling at H.J. Andrews Experimental Forest. *American Meteorological Society* **4**: 251–263.

Waichler SR, Wemple BC, Wigmosta MS. 2005. Simulation of water balance and forest treatment effects at the H.J. Andrews Experimental Forest. *Hydrological Processes* **19**: 3177–3199.

Whitaker A, Alila Y, Beckers J, Toews D. 2003. Application of the distributed hydrology soil vegetation model to Redfish Creek, British Columbia: model evaluation using internal catchment data. *Hydrological Processes* **17**: 199–224.

Wigmosta MS, Vail LW, Lettenmaier DP. 1994. A distributed hydrology-vegetation model for complex terrain. *Water Resources Research* **30**: 1665–1697.

Wigmosta MS, Nijssen B, Storck P. 2002. The distributed hydrology soil vegetation model. In *Mathematical Models of Small Watershed Hydrology Applications*, Singh VP, Frevert DK (eds). Water Resour. Publ.: Highlands Ranch, Colo; 7–42.